JOURNAL OF GEOPHYSICAL RESEARCH, VOL. 105, NO. A11, PAGES 25,079–25,095, NOVEMBER 1, 2000

Particle acceleration and coronal mass ejection driven shocks: A theoretical model

G. P. Zank, W. K. M. Rice, and C. C. Wu

Bartol Research Institute, University of Delaware, Newark

Abstract. There is increasing evidence to suggest that energetic particles observed in "gradual" solar energetic particle (SEP) events are accelerated at shock waves driven out of the corona by coronal mass ejections. Energetic particle abundances suggest too that SEPs are accelerated from in situ solar wind or coronal plasma rather than from high-temperature flare material. A dynamical time-dependent model of particle acceleration at a propagating, evolving interplanetary shock is presented here. The theoretical model includes the determination of the particle injection energy (injection here refers to the injection of particles into the diffusive shock acceleration mechanism), the maximum energy of particles accelerated at the shock, energetic particle spectra at all spatial and temporal locations, and the dynamical distribution of particles that escape upstream and downstream from the evolving shock complex. As the shock evolves, energetic particles are trapped downstream of the shock and diffuse slowly away. In the immediate vicinity of the shock, broken power law spectra are predicted for the energetic particle distribution function. The escaping distribution consists primarily of very energetic particles initially with a very hard power law spectrum (harder than that at the shock itself) with a rollover at lower energies. As the shock propagates further into the solar wind, the escaping ion distribution fills in at lower energies, and the overall spectrum remains hard. Downstream of the shock, the shape of the accelerated particle spectrum evolves from a convex, broken power law shape near the shock to a concave spectrum far downstream of the shock. Intensity profiles for particles of different energies are computed, and the relation between arrival times, maximum predicted energies, and shock propagation characteristics are described. These results are of particular importance in the context of predictive space weather studies.

1. Introduction

Circumstantial evidence which suggests that energetic particles observed in large "gradual" solar energetic particle (SEP) events are accelerated at shock waves driven out of the corona by coronal mass ejections (CMEs) has been accumulating for the last decade (see the reviews by *Reames* [1990, 1995, 1999], *Cane* [1995], *Kahler* [1992], *Dryer* 1994, and *Gosling*, [1993]). The CME origin of energetic particles has proved controversial since it was long thought that solar flares represented the site for gradual SEP events. However, *Kahler et al.* [1984] found that large SEP events and CMEs were very highly correlated (96%), as were SEP intensities and the size and speed of the CME. The spatial and temporal distribution of energetic particles supports the association between SEP events and large, fast CME-driven shocks [see, e.g., *Reames*, 1993, 1999; *Cane*, 1995; and references therein]. In particular, *Reames et al.* [1997], citing previous observations by *McKibben* [1972], have drawn attention to the "invariant" energetic particle spectral shape after the passage of an interplanetary shock driven by a CME. Using multispacecraft observations, Reames et al. observed that the energetic particle spectral shape at different energies, ranging from ~0.03 to 6 MeV/amu, can be invariant over a wide range of heliolongitudes and invariant over time as the shock expands and the downstream intensity declines. These results provide compelling evidence for ion acceleration at the shock.

Energetic particle abundances [*Mason et al.*, 1984; *Cane et al.*, 1986; *Reames and Stone*, 1986; *Tan et al.*, 1986] suggest too that low-energy SEP (approximately several MeV) are accelerated from in situ solar wind or coronal plasma rather than from high-temperature flare material. Since charge states are unaffected by interplanetary transport (solar wind number densities are too low to support additional significant collisional ionization or recombination), one can determine the source of escaping energetic particles by measuring ionic charge states. For impulsive flare events the measured states of Si and Fe indicate that these ions were energized in hot flare plasma ($T \approx 2\times10^7$ K). Gradual SEP events associated with CME-driven shocks suggest instead that the observed energetic ions originated in cooler coronal material ($T \approx 2\times10^6$K) [*Luhn et al.*, 1984, 1987; *Leske et al.*, 1995; *Mason et al.*, 1995; *Tylka et al.*, 1995; *Oetliker et al.*, 1997]. These results are complicated somewhat by observations of particle acceleration [*Mason et al.*, 1999] which suggest that high-energy (several tens of MeV) and low-energy particles may result from different seed and acceleration mechanisms dominating different energy regimes. Nonetheless, the evidence suggests very strongly that ions are accelerated at CME-driven shocks and that the ions can reach energies of several to tens of MeV.

Paper number 1999JA000455.
0148-0227/00/1999JA000455$09.00

While the association between CME-driven shocks and gradual SEP events appears to be clear, the acceleration mechanism underlying this association is much less well understood. The most commonly accepted mechanism for particle acceleration at a shock wave is first-order Fermi acceleration, also known as diffusive shock acceleration [*Axford et al.*, 1977; *Bell*, 1978a, b; *Krymsky*, 1977; *Blandford and Ostriker*, 1978]. Since particles accelerated at the shock escape rather easily from the acceleration site, they can be detected well before the arrival of the shock. This, of course, has immediate and interesting implications for space weather monitoring and prediction systems, but it does imply too that the study of the ion acceleration mechanism is complicated by the subsequent interplanetary propagation of the energetic particles. Furthermore, the site of particle acceleration is likely to be highly turbulent with particles experiencing strong scattering, unlike the less disturbed interplanetary medium into which they escape. Thus the simple application of diffusive shock acceleration theory, which assumes infinitely extended diffusive regions, is not fully correct. The simple diffusion theory assumes too that the shocks are steady and do not evolve in time. The finite size of the shocks is also generally neglected. *Lee and Ryan* [1986] adopted an analytic approach to solve the time-dependent cosmic ray diffusion equation for an evolving interplanetary shock which was modeled as a blast wave. Besides the inapplicability of the diffusion approximation outside the shock region, some strong assumptions were needed to retain a tractable model, in particular, very high blast wave velocities and a radial mean free path which increased with r^2, where r denotes the radial heliocentric distance. Neither assumption is especially well supported observationally in the inner heliosphere.

In view of the complications alluded to above in the diffusive theory of shock acceleration, we plan, in a series of papers, to develop a model of particle energization at evolving or time-dependent CME-driven shocks in the inner heliosphere. In this first report we describe the basic physical model that we implement numerically, and we describe some initial calculations. In constructing the model we assumed that an extended volume element is convected outward in the solar wind. This volume is then subdivided into a series of shells created by a propagating shock. Particles are accelerated locally at the shock by diffusive shock acceleration, producing a local distribution whose spectral characteristics (power law slope and minimum and maximum energies) are determined by the local characteristics of the shock wave (Mach number and compression ratio). A simple injection model is assumed, and the injection intensity is regulated to ensure that the test particle assumption is not violated. The diffusion coefficient at the shock is computed from the wave energy equation which describes wave excitation by the streaming energetic particles. Energized particles then diffuse between shells, and those particles that diffuse far enough upstream of the shock are allowed to escape. For the present, a simple ballistic model for the propagation of energetic particles escaping from the shock is used. In this manner, energetic particle spectra and intensity profiles are produced at all spatial locations for all times upstream and downstream of the interplanetary shock.

In section 2 we develop the basic model to describe particle energization at a propagating shock, describe our approach to determining minimum and maximum particle energies, discuss our determination of the diffusion coefficient, and address some analytic implications of the model. The numerical implementation of our model is also discussed in section 2. Section 3 presents the results from a sample calculation. We conclude with some discussion in section 4.

2. The Extended Dynamical Onion Shell Model

The onion shell model is an empirical approach that was devised to approximate the solution of the cosmic ray transport equation at evolving spherically symmetric supernova remnant (SNR) shock fronts [*Moraal and Axford*, 1983; *Bogdan and Völk*, 1983; *Völk et al.*, 1988]. Although simpler than a full numerical solution, it is a useful approach in that it allows one to appraise the effects of evolving shock strength, spherical geometry, and nonuniform fluid flow on the spectrum of accelerated particles in SNRs. The original onion shell model is essentially nondynamical and cannot provide dynamical accelerated particle spectra as the shock evolves. *Völk et al.'s* [1988] model and earlier models provided the cosmic ray momentum spectrum of all shock-accelerated particles over the entire lifetime of a SNR. L. A. Zank, R. Beck, H. J. Völk, and G. P. Zank (hereinafter referred to as ZBVZ), in unpublished work (1988), extended the original onion shell model by considering the accelerated electron spectrum at an intermediate stage in the lifetime of a SNR. This means, in a sense to be made more precise in section 2.1, that particles accelerated at the shock front experience only incomplete mixing, especially at low energies, within the SNR volume and experience an incomplete adiabatic cooling since the remnant continues to expand. Although the ZBVZ model was nondynamical, it provides a useful precedent for the development of a fully dynamical model.

In sections 2.1-2.5, we shall significantly extend the onion shell models to follow the evolution in space, time, and momentum of an energetic particle spectrum accelerated by a propagating shock in a wind. This model will be used to investigate particle acceleration at interplanetary shocks driven by CMEs in the inner heliosphere.

2.1. Basic Method: Overview

Consider a shock expanding into the solar wind, driven perhaps by a CME. Suppose that M_f is the final shock Mach number of interest for the simulation. We are interested in following the shock for all times $t < t_f$, where t_f corresponds to the time at which the shock Mach number $M = M_f$. The onion shell model approximates the region over which the shock sweeps by a set of concentric spherical (partial) shells, disregarding possible asymmetries introduced by the interplanetary medium. The outer or leading edge of each shell is "created" at the time t when the shock was located at $R(t)$, and the inner part is "created" at an earlier time, $t - \Delta t$. After creation the nested shells evolve (i.e., expand adiabatically and experience convection). At the shock itself the accelerated particle spectrum is obtained approximately by adopting the solution to the full cosmic ray transport equation under the assumption that the time-dependent coefficients can be treated as locally constant and planar, i.e., using the instantaneous shock Mach number and compression ratio. The difficulty in this approach lies in

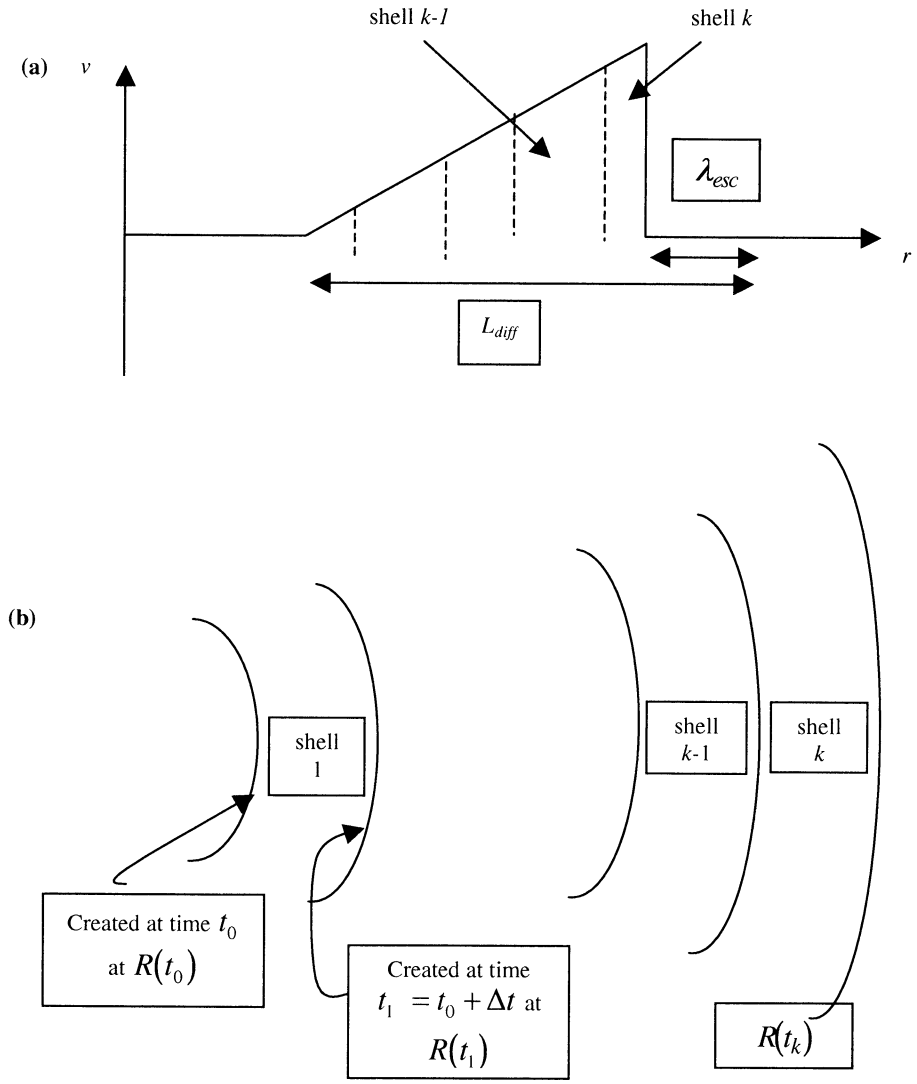

Figure 1. (a) Schematic of the density structure of an interplanetary blast wave. The total structure is subdivided into a series of concentric shells with the most recently formed shells labeled k-1 and k. Two length scales are identified: the escape length scale ahead of the shock front, λ_{esc}, beyond which energetic particles do not scatter diffusively back to the shock, and the scale size of the structure within which energetic ions are transported diffusively, L_{diff}. (b) A related schematic showing the concentric shells and their formation time as the shock propagates into the inhomogeneous solar wind. At time t_k the shock front is located at $R(t_k)$, which creates the edge of the outermost shell, identified as shell k. After formation the shells continue to evolve, being convected with the solar wind and expanding adiabatically.

"patching" together the accelerated particle solutions generated during a series of small, discrete time intervals, and for this the shell concept is useful.

Consider Figure 1. At some time $t_i \le t_f$, the shock is located at $R(t_i)$. The shock generates an energetic particle momentum spectrum $\propto p^{-q(t_i)}$, where p refers to particle momentum and $q(t_i) = 3s_i/(s_i - 1)$ is the familiar power law index for diffusive shock accelerated particles and depends only on the instantaneous shock compression ratio s_i. To this spectrum must be added the preexisting spectrum that diffused into shell i from the other shells (those shells behind shell i and from the region ahead of the shock) created before the shock reached $R(t_i)$. At the same time, t_i, all the shells behind $R(t_i)$ have expanded from their compressed state at time t_{i-1}. The shell expansion is a consequence of both the adiabatic expansion of the plasma after being compressed and heated by the interplanetary shock as well as the shell experiencing convection into a solar wind whose density and temperature decrease with increasing heliocentric distance. Thus, the accelerated particle distribution function in the expanding shells must decompress. The energetic particles in all shells must also diffuse, thus modifying the spectra in all shells since energetic particles from one shell diffuse into neighboring shells while also gaining particles from neighboring shells. In this manner, the temporal, spatial, and momentum distribution of energetic particles accelerated at a propagating interplanetary shock can be determined.

Finally, the region behind and in the vicinity of the

traveling shock is expected to be highly turbulent, with particle transport being essentially diffusive in character. At some distance ahead of the shock, however, the solar wind is much less magnetically turbulent, and particle scattering is significantly weaker. In these regions beyond the shock, particles can propagate subject to weak scattering, so rendering the diffusive approximation invalid [*Ruffolo*, 1997; *Cane*, 1997] (see also *Ng et al.* [1999] and *Tylka et al.* [1999]). To address the difficulty in modeling particle transport through a diffusive environment and then a region of weak scattering, we introduce an escape length scale λ_{esc}. If particles propagate diffusively to some distance λ_{esc} ahead of the shock, we then assume that these particles escape from the shock and stream away from the shock without scattering, never to return. It is these energized escaped particles that will be observed at an observation station prior to the arrival of the shock itself.

In sections 2.2 – 2.5, we expand on the basic model described here, discussing how we model shock propagation, particle spectra, particle injection, determination of the diffusion coefficient, maximum particle energies, and so forth. The basic problem that we need to solve is the well-known cosmic ray transport equation

$$\frac{\partial f}{\partial t}+u\frac{\partial f}{\partial r}-\nabla\cdot u\frac{p}{3}\frac{\partial f}{\partial p}=\frac{1}{r^2}\frac{\partial}{\partial r}\left(r^2\kappa_{rr}\frac{\partial f}{\partial r}\right)+Q, \qquad (1)$$

at, behind, and some small distance ahead of the shock. Here r denotes radial heliocentric distance, f is the energetic particle distribution function, Q is a source term, p is the particle momentum, and κ_{rr} is the radial spatial diffusion coefficient. Beyond λ_{esc} the Boltzmann equation should govern energetic particle transport. Sections 2.2–2.5 describe our approach to solving (1) in the context of the model described above.

2.2. Shock Propagation, Shell Evolution, and the Energetic Particle Spectrum

In our model a CME drives a shock wave from the Sun at time t_0. A spherically symmetric shock is assumed to propagate into the supersonic solar wind, which is expanding radially as

$$n=n_0\left(\frac{r_o}{r}\right)^2, \qquad (2)$$

where n denotes the solar wind number density. The radial solar wind temperature T satisfies a power law

$$T=T_0\left(\frac{r_o}{r}\right)^{\alpha}, \qquad (3)$$

where α can range from 4/3 to ~1.1, depending on the degree of heating assumed for the solar wind. For the present we assume adiabatic heating ($\alpha=4/3$) of the solar wind and model the solar wind numerically using the standard hydrodynamic equations cast in spherically symmetric form. A shock is generated numerically at the inner boundary by increasing the density and flow velocity for a duration of 1 hour while keeping the temperature constant. The propagating shock structure at 0.35 AU is illustrated in Figures 2a – 2c. Not shown in Figure 2 is the reverse shock propagating back toward the Sun while being convected out in the solar wind.

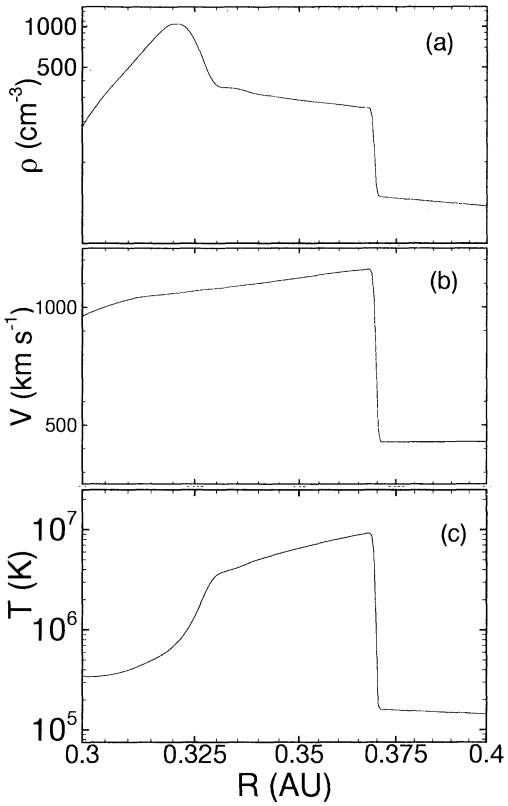

Figure 2. Forward shock structure at ~0.35 AU: (a) density profile, (b) flow velocity, and (c) temperature profile. The reverse shock that terminates the sturcuture is not shown.

In this calculation we consider only acceleration at the stronger forward shock. The structure resembles the sketch of Figure 1 and is typical of a blast wave. Rather than use an analytic prescription to describe the propagation of the shock wave in the inhomogeneous solar wind, as was done by *Völk et al.* [1988], who used a combination of a sweep-up and Sedov-Taylor shock wave, we determine the shock propagation characteristics numerically. This allows us to properly include the solar wind expansion, density and temperature decay with increasing heliocentric distance, and the background wind speed in determining the propagation characteristics of the shock.

It is useful, nonetheless, as we discuss below, to use simple analytic models to describe the propagation of shock waves in order to understand analytically the behavior of the maximum particle energy accelerated at the shock as a function of heliocentric distance and to address the injection threshold energies for thermal solar wind ions. To this end, we can consider a simple sweep-up phase during which the interplanetary shock propagates at an approximately constant velocity $\dot{R}_{SW}=\text{const}$ and whose heliocentric radius increases as $\dot{R}_{SW}t$. After the shock has swept up sufficient mass, a self-similar Sedov-Taylor blast wave solution is assumed to begin. If the end of the sweep-up phase occurs at the radius $R=R_{SW}$ and time $t=t_{SW}$, the Sedov-Taylor solution is approximately $R(t)=(E/\rho_o)^{1/5}t^{2/5}$ for $t>t_{SW}$, where E is the total blast wave energy (typically 5×10^{32} ergs for a CME-driven blast wave) and ρ_0 is a characteristic mass density.

In the earlier onion shell models [*Moraal and Axford*, 1983; *Bogdan and Völk*, 1983; *Völk et al.*, 1988; ZBVZ] the time interval for the supernova shock evolution $[t_o, t_f]$ was divided into n subintervals, $t_0 < t_1 < t_2 < ... < t_{n-1} < t_n = t_f$, and at each time t_k $(k = 0, 1, 2, ...n)$ an imaginary spherical surface with radius $R(t_k)$ was created. The kth shell contained material shocked as the shock wave propagated from $R(t_{k-1})$ to $R(t_k)$ (Figure 1). In the original onion shell models the shock-heated material in the shells was allowed to expand adiabatically back to the ambient interstellar medium (ISM) pressure. Since we consider a dynamical model to determine the accelerated particle distribution at all times, we cannot make this simplifying assumption and must instead compute the shell evolution dynamically. As described above, we model a blast wave propagating into the assumed spherically symmetric solar wind numerically. Consider a shell j created at time t_j, i.e., when the shock was located at $R(t_j)$. The inner edge of shell j is at the same radial distance as the outer edge of shell j-1, which was created at time t_{j-1} when the shock was located at $R(t_{j-1})$ but has since evolved to a new spatial location. This evolution is both as a result of convection in the large-scale solar wind flow and because the postshocked material had an outward velocity. The new location of the outer edge of shell j at time t_i $(i > j)$ is determined from

$$r_j(t_i) = r_j(t_{i-1}) + \int_{t_{i-1}}^{t_i} u(r_j, t')dt', \tag{4}$$

where $u(r_j, t)$ is supplied by the numerical code at successive times. Equation (4) is applied to the edges of all shells created before time t_i. This simple approach allows us to follow the evolution of each shell for all times.

During the time interval Δt_k, taken to be 50 numerical time intervals, while shell k is being created, the shock is assumed to be steady (constant speed, Mach number, and compression ratio). At time t_k (i.e., when shell k is complete) the number of particles, ΔN_k, accelerated during the creation of shell k is

$$\Delta N_k = 4\pi \int_0^\infty p^2 f^n(t_k; t_k, p)dp, \tag{5}$$

where the superscript n reminds us that the distribution function f^n is the number of particles in a unit momentum interval centered on p and not the density of particles. The distribution function $(f^n(t_k; t_k, p))$ is approximated locally by [*Bell*, 1978a; *Krymsky*, 1977; *Axford et al.*, 1977; *Blandford and Ostriker*, 1978]

$$f^n(t_k; t_k, p) \propto p^{-q(t_k)} \left\{ H\left[p - p_{\text{inj}}(t_k)\right] - H\left[p - p_{\max}(t_k)\right] \right\}, \tag{6}$$

where $q(t_k) = 3s(t_k)/[s(t_k) - 1]$ is the spectral index function, $s(t_k)$ is the shock compression ratio at the creation time of the kth shell, p_{inj} is the injection momentum, and $p_{\max}$ is the upper momentum cutoff or the maximum energy that can be achieved locally. Equation (6) is the standard distribution function for the acceleration of particles at a steady, planar shock front. The shock can be assumed to be steady since it does not change significantly in the time Δt_k. The assumption of planarity is valid if $\kappa / V_{sh} < R_{sh}$ (i.e., if the diffusion length scale is much less than the shock radius). As will be seen in section 3, the diffusion coefficient is such that this condition is satisfied. The determination of p_{inj} and $p_{\max}$ is discussed below.

The total number of particles in the kth shell, ΔN_k, is also the product of the injection rate per unit area $Q(t_k)$ times the area of the shock wave, which is typically some fraction of $4\pi R^2(t_k)$, i.e., $\eta 4\pi R^2(t_k)$, where $\eta \le 1$, times the elapsed time Δt_k. We therefore have

$$\Delta N_k(t_k; t_k) = Q(t_k)\eta 4\pi R^2(t_k)\Delta t_k, \tag{7}$$

which provides the normalization for (6),

$$f^n(t_k; t_k, p) = \frac{Q(t_k)\eta R^2(t_k)\Delta t_k}{p_0^3} \frac{3 - q(t_k)}{\left[p_{\max}(t_k)/\, p_{\text{inj}}(t_k)\right]^{3-q(t_k)} - 1} \left(\frac{p_0}{p_{\text{inj}}(t_k)}\right)^{3-q(t_k)} \left(\frac{p}{p_0}\right)^{-q(t_k)} \left\{ H\left[p - p_{\text{inj}}(t_k)\right] - H\left[p - p_{\max}(t_k)\right] \right\} \tag{8}$$

[*Bogdan and Völk.*, 1983; *Völk et al.*, 1988]. Equation (5) gives the number of particles accelerated during the creation of shell k. To obtain the density of particles we must divide (8) by the volume of the shell. Expression (8) therefore allows us to approximate the energetic particle spectrum that is produced at the outermost kth shell by the shock wave located at $R(t_k)$. For simplicity, we neglect the fractional factor related to the actual surface area of the expanding shock, i.e., $\eta \approx 1$. To complete the determination of the local injected particle spectrum, we need to evaluate the lower and maximum limits, p_{inj} and $p_{\max}$, of the power law spectrum.

2.3. Particle Injection at Interplanetary Shocks

The question of particle injection is interesting in terms of its time dependence during the different phases of interplanetary shock evolution. The lowest-energy particles in a newly created shell were accelerated just a short time earlier whereas the highest-energy particles result from a much earlier injection into the Fermi acceleration process. The injection profile in time must therefore play an important role in determining the energetic particle spectrum. In the simplest case the acceleration time, $\tau_{\text{acc}}(p)$, for each momentum p [e.g., *Jokipii*, 1987; *Webb et al.*, 1995] determines the time elapsed since injection occurred. The injected particles themselves have been attenuated during the time $\tau_{\text{acc}}(p)$ since the shock surface has also expanded, distributing the injected and accelerated ions over a larger surface area. Thus, even if one adopts a uniform injection rate per unit area, the later attenuation must have some effect on the accelerated energetic particle spectrum. Only if the acceleration is equal per shell at any epoch do we not have to assume such a dependence.

Let the injection current density $\overline{Q}(p,t)$ at the shock, located at $R(t)$, be given by

$$\overline{Q}(p,t) = n_{\text{inj}} \frac{\delta(p - p_{\text{inj}})}{4\pi p^2} \dot{R}(t), \tag{9}$$

implying that the spatial injection flux density is therefore given by

$$Q(t) = 4\pi \int_0^\infty \overline{Q}(p,t) p^2 dp = n_{\text{inj}} \dot{R}(t) \tag{10}$$

[*Völk et al.*, 1988]. The total flux in phase space across a shell of radius R is

$$\eta 4\pi R^2(t)\overline{Q}(p,t) = \eta 4\pi R^2(t)\dot{R}(t) n_{\text{inj}} \frac{\delta(p - p_{\text{inj}})}{4\pi p^2},$$

which, when integrated over d^3p, gives the spatial injection flux (particles per unit time)

$$4\pi R^2(t)\int \overline{Q}(p,t)d^3p = 4\pi R^2(t)\dot{R}n_{\rm inj}. \quad (11)$$

For an expanding solar wind the effectiveness of ion injection will be reduced by the radial decay in number density upstream of the shock, that is, we may assume that the number of injected particles, $n_{\rm inj}$, scales with solar wind number density, thus

$$n_{\rm inj} = \delta \cdot n_1 \propto (r)^{-2}. \quad (12)$$

In (12), δ denotes the fraction of solar wind ions injected into the acceleration process. Within the inner heliosphere the injection efficiency for interplanetary shocks is ~ 1-4% for thermal solar wind ions [*Gosling et al.*, 1981; *Gloeckler et al.*, 1994], but this can increase significantly in the presence of interstellar pickup ions [*Gloeckler et al.*, 1994; *Fränz et al.*, 1999]. The implication of (11) is interesting. During the decaying phase of interplanetary shock propagation, possibly modeled as a Sedov-Taylor blast wave solution, the spatial injection flux decreases weakly with time ($\sim t^{-3/5}$), whereas the number of injected particles per unit time is constant during the sweep-up phase.

We should, in principle, ensure that particle injection always remains below some threshhold efficiency in order to remain within the test particle limit for the energetic ion pressure [*Völk et al.*, 1988]. This constraint appears to be met always within the solar wind, and so we do not need to introduce an iterative procedure to determine an appropriate level of particle injection at the interplanetary shock. This is a consequence both of the decreasing solar wind density with increasing heliocentric distance and of the relative weakness of most interplanetary shocks. The fact that the constraint is met implies that the test particle assumption is justified a posteriori, and we do not need to include the back reaction of accelerated ions on the dynamical evolution of the shock and accelerated spectrum. Thus, within the context of the sweep-up and Sedov-Taylor approximations, we may conclude that young interplanetary shocks which have not yet experienced any significant deceleration inject and accelerate particles far more efficiently than do older shocks which are in a decaying phase. Furthermore, the highest particle energies result from ions injected during the earlier sweep-up phase.

To determine the injection momentum, we follow *Völk et al.* [1988]. The injection momentum $p_{\rm inj}$ is assumed to be some fraction of the downstream thermal energy per particle. The use of $p_{g2} \equiv 2/3 n_2 p^2(t)/2m_p$ (where p_{g2} and n_2 denote the downstream thermal gas pressure and number density respectively, m_p denotes the proton mass, and p denotes the particle momentum) and the Rankine-Hugoniot condition for energy flux yields

$$p_{\rm inj}(r,t) = \left[\frac{3\alpha m_p(\gamma-1)\rho_1(r)\dot{R}^3(t)}{2\gamma n_2(t)u_2(t)}\right]^{\frac{1}{2}} \left\{1-\left(\frac{\rho_1(t)}{\rho_2(t)}\right)^2 + \frac{2}{(\gamma-1)M_1^2(t)}\right\}^{\frac{1}{2}} \quad (13)$$

where the subscripts 1 and 2 denote upstream and downstream evaluation of the respective quantities. The quantity α is a parameter which is taken to be 0.5. In evaluating (13), we use the upstream and downstream values determined from the numerical code. Of course, the injection model used here is highly simplistic and essentially provides an estimate only for a threshhold energy above which a particle can no longer be regarded as part of the thermal solar wind population. More sophisticated injection models, such as that by *Malkov* [1998], try to identify more precisely how the energized particle distribution emerges from the thermal ion population. The details of these models are not included in our present treatment of ion injection at an interplanetry shock.

2.4. Maximum Particle Momentum Estimate

To compute the maximum particle energy accelerated at a propagating interplanetary shock, $p_{\rm max}$, is more laborious since we attempt to do this as self-consistently as possible. In the vicinity of the shock we assume that the scattering irregularities are Alfvén waves propagating along the mean interplanetary magnetic field **B**. For diffusive shock acceleration to occur at the shock, ions must be scattered rapidly by magnetic fluctuations near the shock. The waves responsible for scattering the ions are assumed to be excited by the energetic ions streaming away from the shock [*Lee*, 1983]. However, ignoring in situ waves convected into the shock from far upstream may not adequately address the scattering of very high energy particles since the linear growth rate due to their streaming is small [e.g., *McKenzie and Völk*, 1982]. This approach is nonetheless consistent with our assumption that the diffusion–convection description of energetic particle transport is limited to the vicinity and downstream of the shock, rather than the more usual assumption of an infinitely extended diffusive regime.

A general determination of $p_{\rm max}$ is described here although we then restrict the computational model to the strong wave field limit. Following *Bell* [1978a] and *Lagage and Cesarsky* [1983], we may solve for the wave energy density, $A(r,k)$, per unit logarithmic bandwidth in wavenumber k, normalized to the energy density in the mean magnetic field, from

$$\frac{\partial A}{\partial t} + u\frac{\partial A}{\partial r} = \Gamma A - \gamma A, \quad (14)$$

where Γ is the wave growth rate and γ is the damping rate. Equation (14) is coupled to the energetic particle transport equation for the distribution function $f(t,r,p)$

$$\frac{\partial f}{\partial t} + u\frac{\partial f}{\partial r} - \frac{p}{3}\frac{\partial u}{\partial r}\frac{\partial f}{\partial p} = \frac{\partial}{\partial r}\left(\kappa\frac{\partial f}{\partial r}\right), \quad (15)$$

where we assume explicitly that the shock and its immediate environs are planar. The coupling of (14) and (15) results from the approximate expression for the spatial diffusion coefficient [*Bell*, 1978a],

$$\kappa(p) = \frac{\kappa_0}{A(k)}\frac{B_0}{B}\frac{(p/p_0)^2}{\sqrt{(m_pc/p_0)^2 + (p/p_0)^2}}, \quad (16)$$

$$\kappa_0 = \frac{4}{3\pi}r_{g0}c = \frac{4}{3\pi}\frac{p_0c}{eB_0},$$

where p_0 is a constant momentum scale, c is the speed of

light, B_0 is a normalizing magnetic field, and r_{g0} is the normalizing ion gyroradius. The linear growth rate for unstable Alfvén waves is given by [*Bell*, 1978a; *Lee*, 1983]

$$\Gamma(k)=\frac{4\pi}{3}\frac{v_A p^4}{A(k)}\frac{c}{\sqrt{(m_p c/p)^2+1}}\frac{2\mu_o}{B^2}\frac{\partial f}{\partial r}. \qquad (17)$$

In (17), $p=eB/k$ is the magnitude of the particle momentum which is in approximate cyclotron resonance with the wave, v_A is the Alfvén speed, and μ_0 is the permeability of free space. The wave damping term γ in (14) is often assumed to be nonlinear Landau damping [*Völk et al.*, 1988], but this is important only for a high beta plasma and then only for slow mode shocks. Within the inner heliosphere, i.e., within the ionization cavity, we may assume that as a lowest-order approximation, $\gamma\approx 0$. The steady state solution to (14)-(17) with $\gamma=0$ was given by *Bell* [1978a]. The localized solution in the upstream region $x<0$ is then

$$A(x,k)=\frac{4}{3\pi}\frac{p}{eB}\frac{c/u_1}{\sqrt{(m_p c/p)^2+1}}(x-x_0)^{-1};$$

$$f(x,p)-f(-\infty,p)=\frac{B^2}{2\mu_o}\frac{r_g}{\pi^2 v_A p^4}(x-x_0)^{-1}, \qquad (18)$$

$$x_0=\frac{(B^2/2\mu_o)(1/\pi^2 v_A p^3)1/eB}{f(x=0,p)-f(-\infty,p)},$$

where $f(x=0,p)$ is the steady state solution of (16) at the shock, $f(-\infty,p)$ is the energetic particle population advected into the shock, and $r_g = p/eB$. The coordinate x refers to the shock-centered frame and is introduced here to distinguish the coordinates from the heliocentric r term. At a strong shock, $f(x=0,p)\sim p^{-4}$, which in this case shows that $A(0,k)$ is independent of k. Furthermore, $A(0,k)$ exceeds unity, in which case the ion scattering mean free path is approximately the particle gyroradius. Since the shocks that are considered in this report are likely to remain reasonably strong in the region of interest (within ~2 AU), we shall accordingly restrict our attention to the limit $A(0,k)\approx 1$ and assume the Bohm form of the diffusion coefficient. Thus $\kappa(p)$ is given by (16) with $A(k)=1$. The model can be extended to shocks of arbitrary strength by solving for the wave energy density when determining the diffusion coefficient.

By equating the dynamical timescale of the shock, $R(t)/\dot{R}(t)$, with the acceleration time scale [*Drury*, 1983], we can determine the maximum ion momentum $p_{\max}$ in the kth shell. Use of

$$\frac{R(t)}{\dot{R}(t)}\approx\frac{q(t)}{u_1^2}\int_{p_{inj}}^{p_{\max}}\kappa(p')d(\ln(p')), \qquad (19)$$

where u_1 is the upstream solar wind speed measured in the shock frame, with equation (16) then yields

$$p_{\max}=\left\{\left[\frac{R(t)u_1^2}{q(t)\kappa_0\dot{R}}\frac{B}{B_0}+\sqrt{\left(\frac{m_p c}{p_0}\right)^2+\left(\frac{p_{inj}}{p_0}\right)^2}\right]^2-\left(\frac{m_p c}{p_0}\right)^2\right\}^{1/2}, \qquad (20)$$

as the upper momentum cutoff. The magnitude of the interplanetary magnetic field $\boldsymbol{B}$ is given by the usual expression [*Parker*, 1958]

$$\frac{B}{B_0}=\left(\frac{R_0}{r}\right)^2\left[1+\left(\frac{\Omega_0 R_0}{u}\right)^2\left(\frac{r}{R_0}-1\right)^2\sin^2\theta\right]^{1/2}, \qquad (21)$$

where θ is the colatitude of the solar wind with respect to the solar rotation axis, Ω_0 is the solar rotation rate, u is the radial solar wind speed, and B_0 is the interplanetary magnetic field (IMF) magnitude at the corotation radius R_0 (typically, $R_0 = 10R_\odot$, $B_0 = 1.83\times10^{-6}$ T, $u = 400$ km/s, and $\Omega_0 = 2\pi/25.4$ days).

Equation (20) reveals explicitly the competition between the shock lifetime and the decaying magnetic field in determining the maximum particle energy to which an ion can be accelerated by an interplanetary shock. Evidently, a higher-velocity shock (u_1 large) can accelerate particles to higher energies than a low-velocity shock can, and older shocks with a larger radius $R(t)$ will produce higher particle energies than a younger shock will provided that $\dot{R}(t)$ does not decay more rapidly than $R(t)$ increases. For a strong shock it is reasonable to assume that $\dot{R}(t)\approx u_1$. Consequently, during the sweep-up phase, $p_{\max}\sim t/r$ (since $B\sim r^{-1}$) whereas during the Sedov-Taylor phase, $p_{\max}\sim t^{-1/5}/r$. Perhaps a clearer way to view the maximum accelerated particle energy is to use $p_{\max}\propto\dot{R}(t)R(t)/r$. Since $R(t)=r$ at the shock location, $p_{\max}\propto\dot{R}(t)$. Thus, in the solar wind, $p_{\max}$ will always decay with time if the shock is decelerating ($p_{\max}\propto t^{-3/5}$ for a Sedov-Taylor shock) unless it is driven and held at a constant speed or if it is somehow accelerating. It is worth noting that only for a constant or increasing magnetic field (such as may occur in the heliosheath or the interstellar medium, for example) and a shock satisfying $R\dot{R}\sim t^\alpha$, $\alpha>0$, can $p_{\max}$ increase with time at a propagating shock. For a weak shock the situation is somewhat more complicated. As the shock weakens, the diffusion coefficient for a given momentum increases ($A(k)$ in (16) decreases as the shock weakens), increasing the acceleration time. Although the dynamical timescale of the shock also increases as the shock weakens, the acceleration time will increase more rapidly, so reducing the maximum energy.

2.5. Transport of the Accelerated Particles

We consider two types of accelerated particles: those that are currently being accelerated and those that have already been accelerated and are resident in the complete shells behind the shock. The particles that are currently experiencing acceleration (i.e., between time t_{k-1} and time t_k) are assumed to obey the steady state diffusive transport equation [*Drury*, 1983; *Zank*, 1999]. Between the leading edge of shell k-1 and the shock front, the particle distribution is constant. Upstream of the shock the particle distribution falls off exponentially with a scale length given by the diffusion coefficient. Beyond a distance λ_{esc} ahead of the shock, the particles are assumed to escape and propagate ballistically along the magnetic field lines away from the shock. The accelerated particle distribution is therefore given by

$$f(t_k;t,r,p)=\begin{cases}0 & r<r_{k-1}(t)\\ Ap^{-q} & r_{k-1}(t)<r<R(t)\\ Ap^{-q}e^{-[r-R(t)]v_{sh}/\kappa(p)} & R(t)<r<R(t)+\lambda_{\rm esc}\\ \dfrac{1}{v\Delta t}\displaystyle\int_{R(t)+\lambda_{\rm esc}}^{\infty}Ap^{-q}e^{-[r-R(t)]v_{sh}/\kappa(p)}dr & r>R(t)+\lambda_{\rm esc}\end{cases}, \quad (22)$$

where A is a normalization factor such that the total number of particles with momentum p is given by (8). $R(t)$ is the position of the shock at time t, $r_{k-1}(t)$ is the position of the leading edge of shell k-1 at time t, and v_{sh} is the shock velocity measured in the upstream frame. The term $1/v\Delta t$ is a length scale associated with the escaping particles, where v is the velocity of the particle of momentum p and Δt is the time between t_{k-1} and t (remembering that t must lie between t_{k-1} and t_k). Equation (22) is written in terms of particle density. In practice, when we keep track of the particle distribution functions in each shell, we consider the number of particles per momentum interval dp in the shell instead of the phase space density of particles in the shell, as that is the quantity that must be conserved.

We also need to consider the fate of ions accelerated at earlier times, $t<t_{k-1}$. The energetic particles located in all the shells created prior to $t=t_k$ obey the time-dependent transport equation (1). This is difficult to solve in a restricted region, so we approximate the solution of (1) term-by term, as follows.

To solve (1) we use a technique analogous to operator splitting and separate it into three parts. Consider an energetic particle population in shell i at time t_{k-1}. During the time interval $\Delta t=t_k-t_{k-1}$ the particles convect with the shell, whose inner and outer boundaries are now located farther out in the solar wind (a combination of convection in the background solar wind and expansion of the shell). Thus, for $t\in[t_{k-1},t_k]$ we have, for the first part of the split,

$$\frac{\partial f}{\partial t}+u\frac{\partial f}{\partial r}\approx 0. \quad (23)$$

At time t_{k-1}, $f=f_i(t_{k-1})=f_i[r_i(t_{k-1})]$ in shell i (see Figure 3). The new location of shell i at time t_k is given by (4) and $u[r_i(t),t]$ is supplied numerically from the shock propagation code at successive times (remembering that $r_i(t)$ is the location of shell i at time t). Thus, solving (23) yields

$$f_i(t_k)=f_i\left\{r_i(t_k)-\int_{t_{k-1}}^{t_k}u[r_i(t)]dt\right\}, \quad \left(=f_i\left\{r_i(t_k)-u[r_i(t_k)](t_k-t_{k-1})\right\}\right) \quad (24)$$

where the latter equality holds if the fluid velocity u is constant between t_{k-1} and t_k.

The second part of the split to be updated is

$$\frac{\partial f}{\partial t}-\nabla\cdot u\frac{p}{3}\frac{\partial f}{\partial p}=0. \quad (25)$$

If we introduce $\xi=\ln p$, (25) is equivalent to the system of characteristic equations

$$\frac{d\xi}{dt}=-\frac{1}{3}\nabla\cdot u=-\frac{1}{3}\left(\frac{2u}{r}+\frac{\partial u}{\partial r}\right), \quad \frac{df}{dt}=\text{const}, \quad (26)$$

which yields

$$\xi(t_k)-\xi(t_{k-1})=-\frac{1}{3}\int_{t_{k-1}}^{t_k}\frac{2u}{r}dt-\ln\left[u(t_k)/u(t_{k-1})\right]^{1/3}, \quad (27)$$

subject to the assumption of spherical symmetry (and since u is assumed to be constant between t_{k-1} and t_k, reduces to $\ln p(t_k)=\ln p(t_{k-1})-1/3\nabla\cdot u(t_k-t_{k-1})$ during the interval $[t_{k-1},t_k]$). To compute the first integral in (27), we use (4) to update r at each Δt.

The third part of the split to be updated is

$$\frac{\partial f}{\partial t}=\frac{1}{r^2}\frac{\partial}{\partial r}\left(r^2\kappa\frac{\partial f}{\partial r}\right). \quad (28)$$

Prior to diffusion (at time t_{k-1}), we assume that the particles in each shell are distributed as a broadened delta function with length scale κ/u_1 (u_1 being the upstream fluid speed in the stationary shock frame),

$$f_i(t_{k-1},p,r)=\frac{1}{\sqrt{\pi}(\kappa/u_1)}\frac{f_i^n(t_{k-1},p)}{4\pi r_i(t_k)r}\exp\left[-\frac{\left[r-r_i(t_k)\right]^2}{(\kappa/u_1)^2}\right], \quad (29)$$

where $f_i(t_{k-1},p,r)$ is the number density of particles in shell i at position r, while $f_i^n(t_{k-1},p)$ is the number of particles in shell i (per unit momentum interval centered on momentum p). Since convection of the shells is treated separately (equation (24)), the position of shell i at time t_k ($r_i(t_k)$) can be used in (29) together with the particle's distributions at the earlier time t_{k-1}. In principle, $4\pi r^2$ could have been used in the denominator in the place of $4\pi r_i(t_k)r$. However, the use of $4\pi r^2$, together with the substitution discussed below, produces an equation that diverges as $r\to 0$ and hence is not analytically solvable. Using $4\pi r_i(t_k)r$ conserves particle number and allows us to solve the diffusion equation analytically, and the result is only very slightly different from using $4\pi r^2$ as r remains close to $r_i(t_k)$ for all significant values of the broadened delta function. In using (29), we have made the assumption that the shells are broader than the diffusion length scale κ/u_1, which appears to work well in practice.

Using the substitution $F=rf$, (28) can be rewritten as

$$\frac{\partial F}{\partial t}=\kappa\frac{\partial^2 F}{\partial r^2}. \quad (30)$$

With time, energetic particles in one shell must diffuse into neighboring shells in a momentum-dependent manner. Thus, at some point r at time t, one expects to observe a weighted distribution of the infinitesimal contributions $df(t_i;t,p)$ of each shell at a given momentum. We must therefore introduce a weighting or influence function to model the propagation properties of the energetic particles residing in each shell. For each shell i we diffuse the pre-existing population of ions according to (28) and then simply add the diffusing energetic ion component that originates from the remaining shells and the shock source to what remains.

From (29) the initial condition for F_i is

$$F_i(t_{k-1},p,r)=\frac{1}{\sqrt{\pi}(\kappa/u_1)}\frac{f_i^n(t_{k-1},p)}{4\pi r_i(t_k)}\exp\left[-\frac{\left[r-r_i(t_k)\right]^2}{(\kappa/u_1)^2}\right]. \quad (31)$$

We may use the Green's function for F determined from (30),

$$G(r-r',t-t')=\frac{1}{\sqrt{4\pi\kappa(t-t')}}\exp\left[-\frac{(r-r')^2}{4\kappa(t-t')}\right], \quad t>t', \tag{32}$$

to find the distribution of the shell i ions after diffusion,

$$f_i(t_k,p,r)=F_i(t_k,p,r)/r;$$

$$F_i(t_k,p,r)=\frac{1}{\sqrt{\pi}}\frac{f_i^n(t_{k-1},p)}{4\pi r_i(t_k)}\frac{1}{\sqrt{4\kappa(t_k-t_{k-1})+(\kappa/u_1)^2}} \tag{33}$$

$$\exp\left[-\frac{[r-r_i(t_k)]^2}{4\kappa(t_k-t_{k-1})+(\kappa/u_1)^2}\right].$$

The number of particles that diffuse from shell i into shell j (j can equal i) is then given by

$$f_j^n(t_k,p)=\sum_{r=r_{j-1}(t_k)}^{r=r_j(t_k)} f_i(t_k,p,r)4\pi r^2 dr, \tag{34}$$

where dr is the grid spacing of the numerical code used to model the shock propagation, and not the shell width. The above procedure is repeated for all shells, and the ions in shell j at time t_k will be made up of ions originating from a number of different shells. The range of shells from which these ions have originated depends on their momentum, since the diffusion coefficient κ is a function of momentum p and (28) reflects the greater mobility of more energetic particles than less energetic ions.

To summarize, the distribution of particles accelerated at the shock between times t_{k-1} and t_k is given by (22). At time t_k we assume that shell k is formed with an outer boundary at $R(t_k)$ and an inner boundary at $r_{k-1}(t_k)$, and we suppose that all newly accelerated particles between $r_{k-1}(t_k)$ and $R(t_k)+\lambda_{\rm esc}$ now reside within this shell. Up to a distance $\lambda_{\rm esc}$ ahead of the shock at a given time, we know the exact distribution of the accelerated ions throughout the region through which the shock has propagated. Furthermore, $\lambda_{\rm esc}$ is momentum dependent and therefore of variable length. Thereafter, at the next time step the entire shock structure is evolved through the particle precursor structure ahead of the shock, and we then assume that the particles that were in the diffusive region ahead of the shock are assimilated into the shell in which they were accelerated originally. This is a simple way of ensuring that particle number is conserved. In principle, we could have included some of the precursor particles into the newly created shell, but this is essentially unnecessary for two reasons: firstly, the error introduced by our present procedure is very small (the number densities ahead of the shock being much lower than those behind), and secondly, the more energetic particles have large diffusive mean free paths, and they are not very easily trapped in any single shell.

For shells $i<k$ we use (33) to diffuse the ith shell distribution throughout the region of interest, and we then use (34) to update the energetic particle distribution in each shell (including shell i and k). This is repeated for all $i<k$.

Finally, we define an escape length scale

$$\lambda_{\rm esc}(t_k,p)\equiv a\frac{\kappa(p)}{\dot{R}(t_k)} \tag{35}$$

where a is a constant which we have taken to be 4. The choice of 4 is based on observations which show momentum-dependent exponential increases in intensity upstream of interplanetary shocks. The observed intensity at shock passage can be ~ 50 – 100 (4 – 5 e-foldings) times that prior to the start of the exponential rise (W. Dröge, private communication, 1999). Energetic ions that propagate to a distance of at least $\lambda_{\rm esc}(t_k,p)$ ahead of the shock position (using either equation (34) or equation (22)), which is located at $R(t_k)$, are allowed to escape upstream and never return to the shock or the postshock plasma. Instead, these particles stream away from the acceleration region following the IMF lines. For the present we assume an exceedingly simple interplanetary model for particle propagation in that we simply allow particles to propagate along the field at a speed corresponding to their energy. This may be justified in terms of a telegrapher equation description for ion propagation which assigns to all particles the speeds $\pm v/\sqrt{3}$. In a subsequent paper we will use a direct Boltzmann equation description for particles escaping from the shock.

3. Results

By way of example, we introduce a high-speed shock wave at ~0.1 AU in the numerically computed solar wind. The initial shock speed is ~1500 km/s (Figure 4) and decays rather slowly initially. At ~0.45 AU the shock speed begins to decrease more rapidly than before, slowing to ~820 km/s by 2

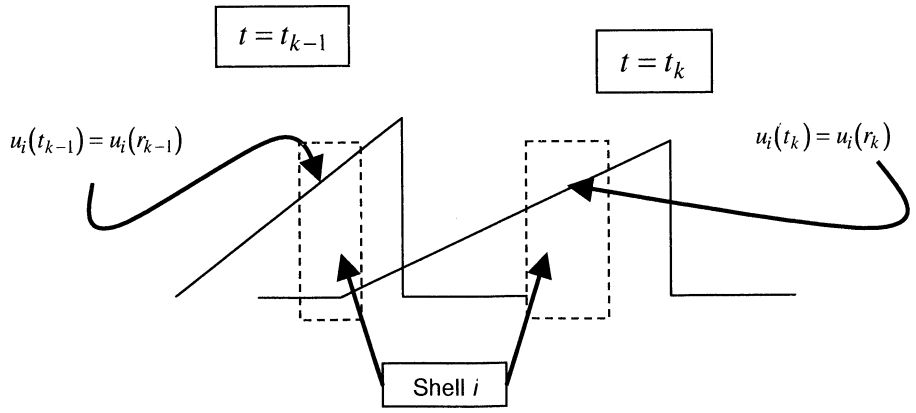

Figure 3. Schematic showing the evolution of a typical shell i from time $t=t_{k-1}$ to time $t=t_k$, illustrating both the effects of convection and adiabatic expansion of the shell.

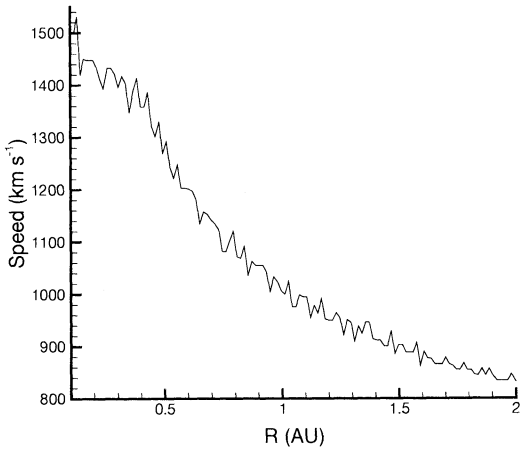

Figure 4. Numerically computed shock speed plotted against radial distance. The shock starts with a speed of ~1500 km/s at 0.1 AU, decreasing to ~900 km/s at 2 AU.

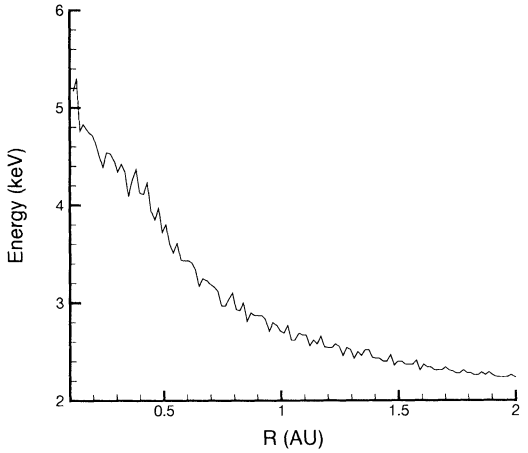

Figure 6. Injection energy plotted against radial distance. Since the shock has a large Mach number, and hence compression ratio, the injection energy does not change significantly. It decreases from a maximum of ~ 5 keV at 0.1 AU to ~ 2.3 keV at 2 AU.

AU, which is roughly twice the solar wind speed. Apart from a difference in magnitude, the shock speed profile is very similar to that shown in Figure 3 of *Cane* [1995]. The fast magnetosonic Mach number, $M(t)$, of the shock is plotted in Figure 5 and shows that $M(t)$ increases until ~0.5 AU after which it is approximately constant with $M(t)$ ~ 10. This, of course, reflects the adiabatic cooling of the solar wind and the dominance of the IMF with increasing heliocentric distance. Since $M(t)$ >> 1 everywhere, the shock compression ratio remains nearly 4 for all heliocentric distances considered here. This has the obvious implication that the accelerated particle spectrum in the leading shell remains hard with $f \sim p^{-4}$. Had the shock been slower, the compression ratio would be smaller and, as we discussed in section 2.2, the accelerated spectrum in the leading shell would be softer, the wave power would be reduced, and the Bohm limit would not apply. Instead, we would compute $A(k)$ at each time interval to determine the momentum-dependent spatial diffusion coefficient. The model that we have developed is therefore applicable to interplanetary shocks of arbitrary strength.

The injected particle energy does not vary greatly from 0.1 to 2 AU, ranging from ~5 keV intially to ~3 keV eventually (Figure 6). This behavior too reflects the large, relatively constant Mach number, and hence compression ratio, of the interplanetary shock. By contrast, the maximum accelerated particle energy at the propagating shock decreases sharply with increasing heliocentric radius. With a maximum energy of a few GeV at early times, maximum energies of ~100 MeV are achieved when the shock is at 2 AU. As discussed in section 2.4, the reduction in the cutoff energy is a result of the actual shock velocity and the IMF strength at a given location. Since both decrease with increasing heliocentric distance from the Sun, particles with the highest energies were accelerated at earlier times when the shock was closest to the Sun (Figure 7). However, as we discuss below, some of the most energetic ions can remain trapped behind the shock, only escaping and propagating upstream at later times. We emphasize that particle energies of order 1 GeV can be achieved by diffusive shock acceleration at strong interplanetary shocks.

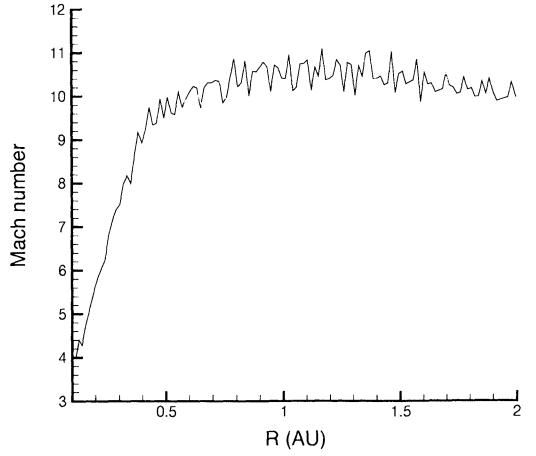

Figure 5. Radial evolution of fast magnetosonic Mach number.

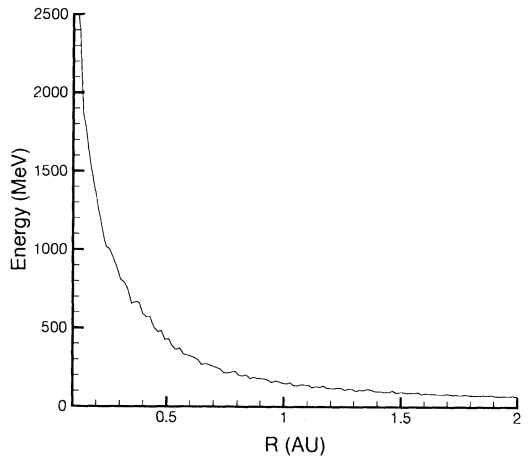

Figure 7. Maximum particle energy versus radial distance. At small radial distances, where the magnetic field is large and the shock speed is high, the maximum energy is of order 1 GeV. As the shock propagates out into the weakening magnetic field, the maximum energy drops rapidly, tending to a few times 10 MeV at 2 AU.

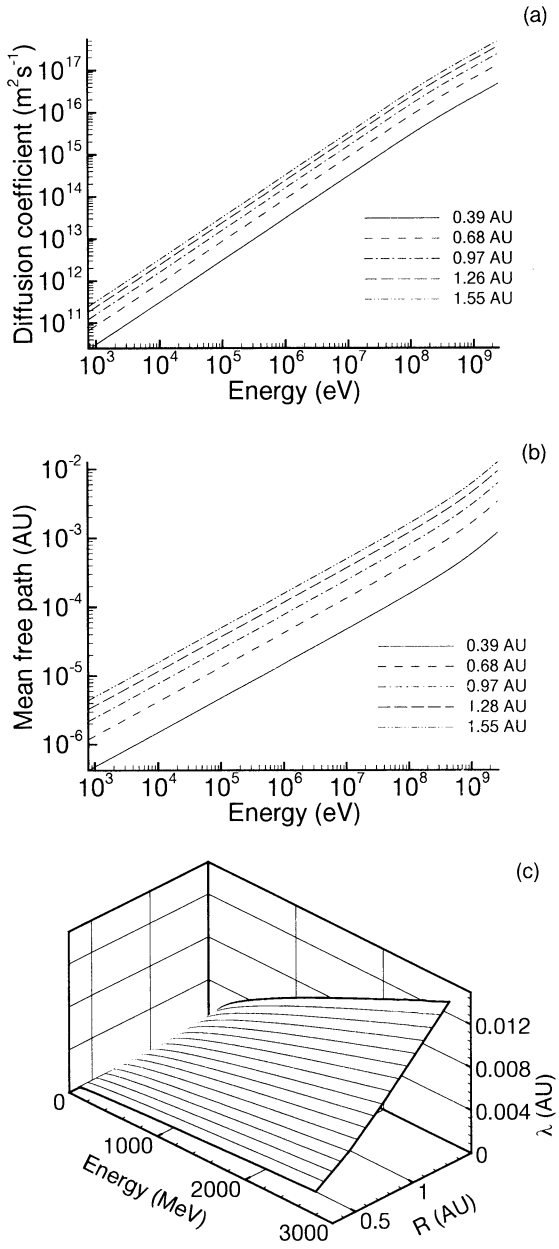

Figure 8. (a) How the diffusion coefficient varies with energy at different radial distances. (b) How the mean free path varies with energy at different radial distances. (c) A three-dimensional plot of Figure 8b. Since the shock in this particular case is strong, the wave energy density is such that the diffusion coefficient is given by the Bohm limit.

The diffusion coefficient and radial mean free path (mfp), $\propto \kappa/v$, are plotted as functions of energy at different radial distances in Figures 8a and 8b. Figure 8c is a three-dimensional plot of Figure 8b. The mfp increases approximately as a power law with energy and more slowly (approximately linearly) with increasing heliocentric distance. The diffusion coefficient and mean free path at the shock are significantly smaller than typical interplanetary values, by nearly 2 orders of magnitude at 1 MeV. Although somewhat smaller than values observed at an interplanetary shock at 1 AU [*Terasawa et al.*, 1999; *Shimada*, 1998], the diffusion coefficient/mean free path values computed in the Bohm limit appear to be reasonable for the strong shock modeled here. The smallness of the diffusion coefficient at the shock compared to typical interplanetary values emphasizes the difficulty in using a simple diffusive transport equation for energetic particles throughout the inner heliosphere. The small diffusion coefficient also allows us to use a planar shock approximation.

The radial and temporal evolution of the accelerated energetic particle spectrum is illustrated in Figures 9 and 10. Figure 9 shows the distribution function observed at 0.5 AU for different times (i.e., as the shells convect past the observer at 0.5 AU). The legend in Figure 9 gives the shell in which the distribution was resident (shells with larger numbers were created more recently) and the time at which the distribution was observed. The time is measured with respect to the initiation of the shock at 0.1 AU. The earliest time (largest shell number) corresponds to the particle distribution in the shell created with the arrival of the shock at 0.5 AU. The later times refer to the postshock particle distribution as it is convected and diffused through the nominal observation point at 0.5 AU. An E^{-2} line is drawn to guide the eye. The most recent accelerated distribution function (the thin solid line of Figure 9) is apparently close to a power law distribution in energy with slope –2, consistent with acceleration by a strong shock, together with a "knee"-like feature at the highest energies. However, closer examination on a smaller scale reveals interesting deviations of the energetic ion spectrum from a simple power law. The most recently created energetic spectrum, resident in shell number 24, is flat at lower energies (30-800 keV) before steepening. Such a "broken" power law distribution was described briefly by *Reames* [1999] and an energetic particle spectrum observed upstream of an interplanetary shock was shown (his Figure 3.3). The convex form of the distribution is understood easily and reflects the greater mobility of the more energetic particles which are able to escape more readily into the interplanetary medium ahead of the shock never to return. The ions escaping from shell 24 are partially replaced by very energetic particles accelerated at earlier epochs when the magnetic field was stronger (Figure 7). The very energetic particles created at earlier

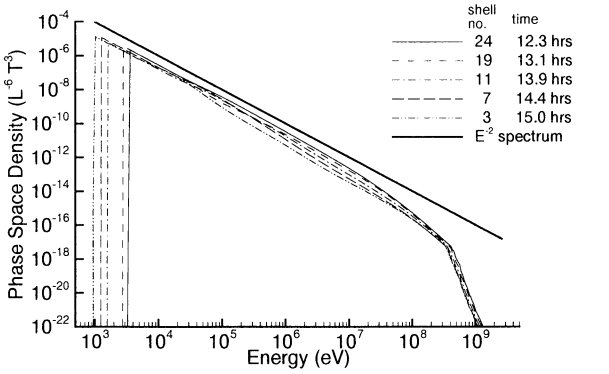

Figure 9. Particle distribution functions observed at 0.5 AU as the shells convect past the observer. The legend gives the shell number (higher number shells were created more recently) and the time at which that shell reached 0.5 AU. The times are measured with respect to the shock initiation at 0.1 AU. A "knee" like feature can be seen at the highest energies.

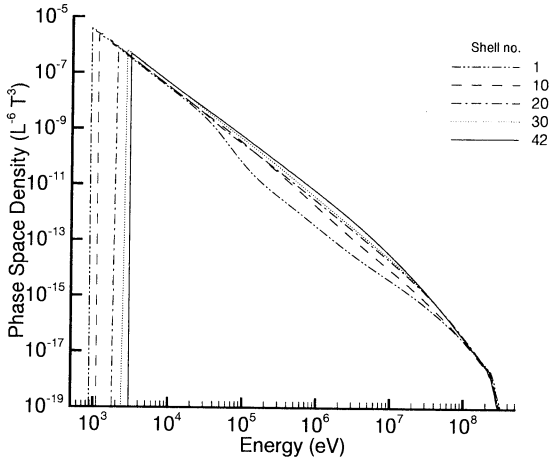

Figure 10. Particle distributions at and behind the shock 20 hours after the shock was initiated at 0.1 AU. At this time the shock is at a radial distance of ~0.72 AU, which is therefore also the approximate position of shell 42. The other shells are all older than shell 42 and are at smaller radial distances.

times were trapped in the postshock flow and can diffuse into neighboring shells at later times. However, the number density of these highly energetic particles is very small, and their presence is observed primarily in the creation of an energetic "knee"-like feature.

The subsequent evolution of the accelerated ion distribution at 0.5 AU is illustrated in the remaining spectra shown in Figure 9. As the older shells are convected out in the solar wind (whose density and temperature are decreasing), they expand adiabatically, and the embedded energetic particle distribution cools. The cooling of the accelerated ion distribution, as shown formally by (27), amounts effectively to shifting the distributions of Figure 9 downward and leftward in the log-log plots. Thus, at the later time when shell 19 has been swept out to 0.5 AU, the minimum and maximum ion energies are smaller than those observed in shell 24 at 0.5 AU (even though when shell 19 was created, $p_{\max}(\text{shell} = 19) > p_{\max}(\text{shell} = 24)$, Figure 7). From Figure 9 it is clear that the spectra progress from a convex shape in the newest shells (shell 24) to a concave shape in the oldest shells. At the lowest energies (below ~ 10 keV) the particles are effectively trapped within their shells and essentially undergo cooling and convection while maintaining the same spectral slope. At the highest energies (above ~ 50 MeV) the diffusion coefficient is such that it is reasonably easy for particles of these energies to escape. Those that do not escape are able to diffuse across a significant region of the postshock flow. The escape of these particles reduces the number trapped behind the shock while the diffusion within the postshock flow effectively averages the intensity in all the shells. As is clear in Figure 9, the phase space density above ~ 50 MeV is very similar in all the shells. This averaging at these high energies produces densities that are lower than those expected in the newest shells but higher than those expected in the oldest shells. The newer shells therefore have a convex profile while the older shells have a concave profile. The concavity of the older shells is further enhanced by the loss of intermediate-energy (between 10 keV and 50 MeV) particles out of the postshock flow in the downstream direction. These intermediate-energy particles are only able to diffuse across a few neighboring shells, and hence the reduction is greatest in the shells near the lower boundary.

In Figure 10 we plot the distribution function at a given time for different spatial locations at and behind the shock. Evidently, the results are closely related to those described above for Figure 9. The distribution in the most recently created shell (shell 42) has a slightly convex, "broken" power law shape. The distributions then progress from this "broken" power law shape in the newest shells to a more concave shape in the oldest shells in the same way as in Figure 9 and for the same reasons.

The omnidirectional spectrum that escaped from the shock complex and propagates to 1 AU on a fixed magnetic field line is displayed in Figure 11 for various times after the shock was launched. Figure 11 should be interpreted somewhat cautiously since, as discussed above, we have not attempted to model the propagation characteristics of the escaped particle distribution with anything more complicated than a telegrapher-like propagation model. Between time t_{k-1} and t_k, particles are accelerated at the shock and diffuse from the shells located behind the shock. Those that diffuse more than an escape length ahead of the shock or that diffuse out behind the postshock flow are allowed to escape and propagate ballistically at speed v. During this time interval we are only able to calculate the number of particles that escape and do not really know their phase space density. To determine their density we need to know the volume that they occupy or, equivalently, we need to know a length scale. Since we assume that they propagate at speed v, the only length scale avaliable is $v(t_k - t_{k-1})$, which is almost certainly too large. For the purposes of Figure 11 it is probably reasonable. We expect the length scale to increase with energy, as ours does. We are also interested in comparing spectra at different times which should not depend on the choice of length scale.

Four hours after t_0 (time of shock initiation), the maximum particle energy is ~1 GeV, and there is evidence of a "knee" (solid line). Above 10 MeV the energetic particle number density as a function of energy is almost a hard power law. It is, however, slightly softer at the lower energies than at the

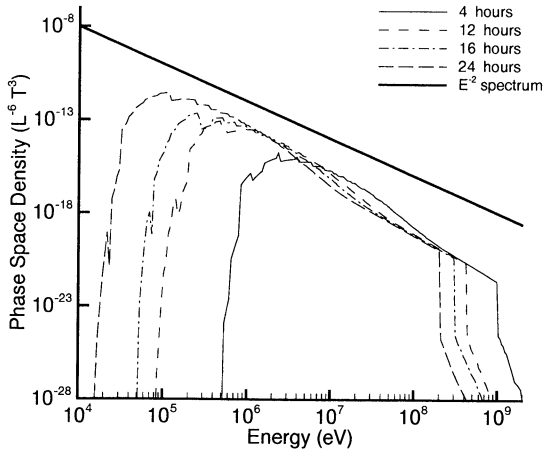

Figure 11. Particle distributions observed at 1 AU, at different times, prior to the shock arrival. Time is measured with respect to the initiation of the shock at 0.1 AU. An E^{-2} spectrum is included to guide the eye.

higher energies. This illustrates the ease with which the high - energy particles escape, compared to the difficultly experienced by the lower-energy particles. Below 10 MeV, the spectrum is rounded. Minimum energies observed are ~0.5 MeV. The diffusion coefficient of these lower-energy particles is such that very few are able to diffuse ahead of the shock and escape; hence the rounded nature of the spectrum at these energies. As the shock approaches, or equivalently, as time increases beyond t_0, increasing numbers of lower-energy ions and fewer very high-energy ions arrive at 1 AU. The spectra are still rounded at the lower energies and are concave power laws at the higher energies. The spectral index does not change significantly, which is an indication that most of the observed particles escaped just after being accelerated. Since the observed particles were not trapped for any significant length of time behind the shock, they did not experience any significant cooling or mixing. As time progresses, the maximum energy of the particles on the power law portion of the spectrum tends to converge to a value of a ~200 MeV. This is consistent with Figure 7, which shows that the maximum energy when the shock is between 0.75 and 1 AU is ~ 200 MeV.

The distribution function of accelerated particles with a given energy as a function of radial distance is plotted in Plate 1. Plate 1 has several curves plotted, which are ordered as follows. The rows of curves are ordered with respect to increasing particle energy: the top correponds to 15 keV particles, and the bottom corresponds to 75 MeV particles. Each column corresponds to a single time. Thus the second column shows the radial distribution of energetic particles at and behind the shock when it was located at $R \sim 0.25$ AU. At this time there were only eight shells, and for each energy the number density peaked at the shock itself. During such early times, the shock and shells are embedded in an IMF which is still sufficiently strong as to ensure that the diffusive length scale at these energies is smaller than the shell extent, thus effectively confining particles of the energies illustrated in Plate 1 to their shells. The particles are also experiencing decompression as they convect out with the solar wind, and hence those trapped in the earliest shells will have a lower phase space density than those in the more recent shells. This profile is maintained for the 15 and 316 keV particles out to beyond 1 AU. This illustrates that at these energies the particles are effectively trapped within their shells and are simply undergoing cooling as they convect with the solar wind. At 17 and 75 MeV, however, the profiles start to roll over. At 75 MeV the profile is almost flat by 1 AU. Even though cooling is also taking place at these energies, their diffusion coefficients are large enough that particles diffuse across a significant portion of the postshock flow, mixing the particle densities. At 17 MeV, diffusion is not large enough to completely flatten the profile.

Finally, we may consider the phase space density profiles predicted from the model described here. As discussed above, we neglect the complications associated with a detailed transport model, such as those developed by, for example, *Kallenrode and Wibberenz* [1997], *Ruffolo* [1995], and *Ng et al.* [1999]. These authors assume an input particle spectrum and then compute the resultant transport to 1 AU. However, unlike the model presented here, no self-consistent determination of the time-dependent shock-accelerated particle distribution is made in the transport codes of Kallenrode and Wibberenz, Ruffolo, and Ng et al. In this respect, our results and their results are complementary. Subject then to these caveats and our neglect of focusing and adiabatic expansion, we obtain the phase space density profiles illustrated in Plate 2. Profiles of particles at five different energies are shown, ranging from 177 MeV (pink filled circles) to 16 keV (red filled squares). The duration of the event is nearly 3 days, corresponding to the launch of the numerical shock at ~0.1 AU until $r = 2$ AU.

As would be expected, the higher-energy particles arrive first. The 177 and 46 MeV particles arrive only minutes after the shock is launched, after which their profiles are almost flat until they jump and increase exponentially in density. The jump begins when the distance from the observation point (1 AU) to the shock is equal to the escape length. Since the escape length depends on the diffusion coefficient, which is energy dependent, it is greatest for the highest-energy particles and smallest for the lowest-energy particles. The escape lengths for the 322, 43 and 16 keV particles are so short that they are not visible in Plate 2. The density jumps in the keV profiles at ~1.3 days occur when the shock arrives at the observation point. In reality, one would not expect the 177 and 46 MeV densities to have the discontinuous jumps shown in Plate 2. These jumps are the result of our very simple escape model for which we are only able to determine the total number of escaped particles. As discussed in section 2.5, we do not know the length scale needed to determine the particle density, and so use $v(t_k - t_{k-1})$ as a first approximation. For 177 MeV particles and for the shell creation times used in our model, this can be as large as 4 AU, which is almost certainly too large. The only other length scale we have is the mean free path within the postshock flow, shown in Figures 8b and 8c. For 177 MeV particles this is $\sim 10^{-3}$ AU and is clearly too low. A length scale of ~0.1 AU would almost remove the discontinuous jump and is probably a good first guess at the mean free path upstream of the shock structure. In the future it is planned to use a full propagation model to model the propagation of escaped particles from the shock to the observer.

After the discontinuous jumps, the 177 and 46 MeV profiles increase exponentially in phase space density. This is the upstream profile for particles accelerated at a steady, planar shock. For the 177 MeV particles this exponential increase ends before the shock arrives at 1 AU and the phase space density starts to decrease. This is because the shock is no longer accelerating particles of this energy (see Figure 7). There remain, however, particles with this energy trapped behind the shock, and hence the density decreases reasonably slowly as these particles escape from the postshock flow. Figure 7 shows that 46 MeV particles are accelerated well beyond 1 AU, and an equivalent decrease in phase space density is not seen. The exponential increase in the density of 46 MeV particles upstream of the shock does, however, turn over slightly before the shock arrives. This is the result of particle diffusion from shells behind the shock into the region ahead of the shock. Comparison of (22) and (33) shows that the phase space density profile of particles that diffuse from shells behind the shock is different from that of the accelerated particles, hence the slight change in the profile just before the arrival of the shock. The 322, 43 and 16 keV phase space density profiles all show discontinuous jumps when the shock arrives at the observation point. As mentioned earlier in this section, this is because their escape length scale is too short to be visible on this plot. As

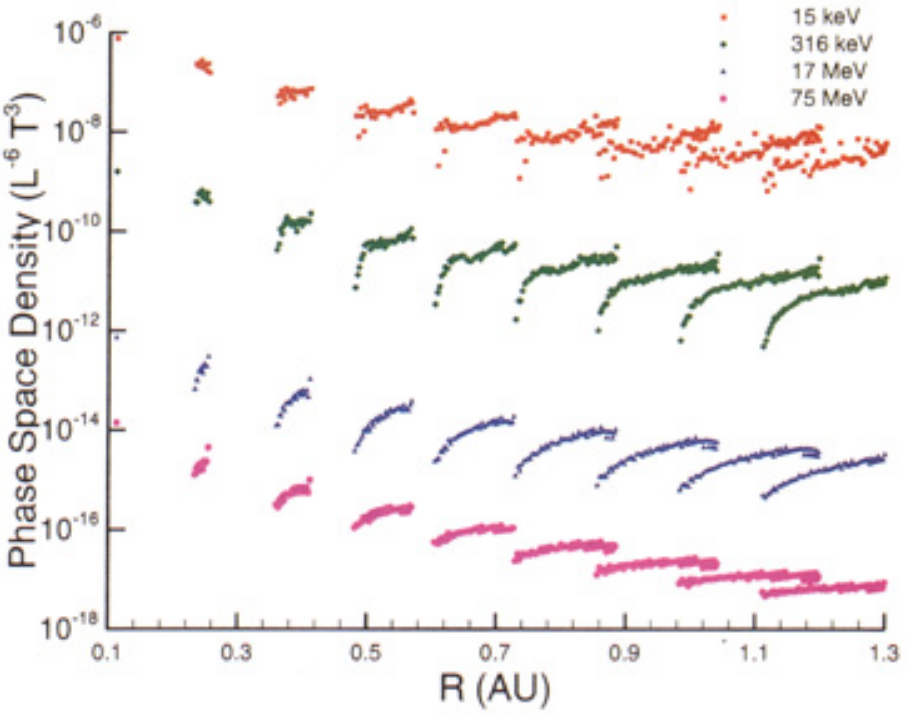

Plate 1. The temporal evolution of the particle intensities in the shells for four different energies. Each point is the intensity in a particular shell, and each group of points represents the intensity in all the shells at a given time. It is clear that as time increases, the number of shells increases. At the lower energies, cooling decreases the intensity in the oldest shells while at the higher energies the larger diffusion coefficient mixes the particles in the different shells, producing a more constant intensity profile.

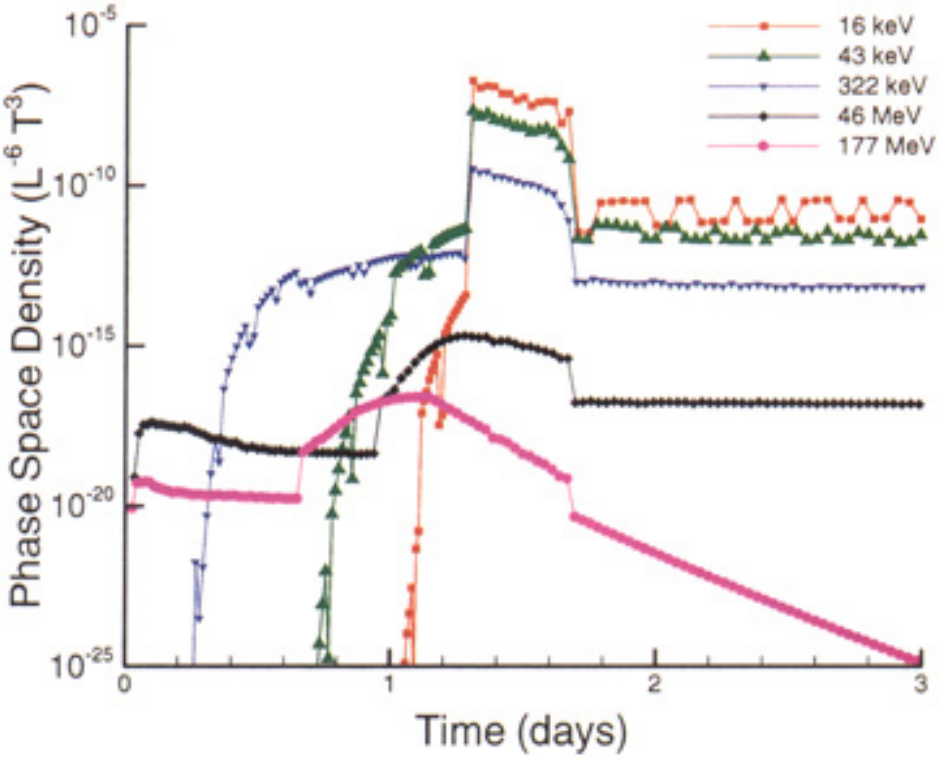

Plate 2. The temporal evolution of the intensity profile observed at a given location (1 AU) at 5 different energies. The shock arrival time is ~ 1.3 days after its injection at 0.1 AU.

expected, the 322 keV particles arrive first, followed by the 43 keV particles, and finally by the 16 keV particles. Before the arrival of the shock, the density of the 16 keV particles is always less than that of the 43 and 322 keV particles. This is because it is extremely difficult for particles of this energy to diffuse upstream of the shock, and so the density of escaped particles is always extremely low compared to the density of particles trapped in the postshock flow. After the shock has passed the observation point, the 16 keV density jumps up above the 43 and 322 keV densities. These phase space densities then all show gradual decreases until the entire postshock flow has moved past the observer. The decreases result from cooling of the trapped distributions which reduces the density at these energies. After the postshock flow has convected beyond the observation point, all five profiles show a discontinuous jump down to a lower density. These are particles which have escaped downstream from the shocked material and are now propagating back to the observer. As with the upstream escaped particles, we must assume a (probably too large) length scale.

4. Concluding Remarks

Gradual SEP events are now thought to be the result of particle acceleration at interplanetary shock waves, often driven by CMEs. This has stimulated several theoretical and modeling efforts. In particular, *Heras et al.* [1992, 1995], *Lario et al.* [1998], *Kallenrode and Wibberenz* [1997], and *Kallenrode and Hatzky* [1999] have attempted to fit energetic proton events to models by assuming that ions are "injected" into the interplanetary medium at a moving source (the propagating shock). (We emphasize that our use of the term injection in this report is entirely different from the sense in which it is used by Heras et al., Lario et al., Kallenrode and Wibberenz, and Kallenrode and Hatzky, see our section 2.3. A closer analogy is with our use of the term "escape.") These authors then solve the Boltzmann equation numerically to model the subsequent transport of the particles from the shock to an observation point. By fitting the observed ion flux and first-order anisotropy profiles to models, Heras et al., Lario et al., Kallenrode and Wibberenz, and Kallenrode and Hatzky then attempt to determine the characteristics of both the accelerated ion source $Q(r,t)$ and the parallel mean free path. While this approach is certainly of interest and value, it does not address the fundamental nature of particle acceleration at evolving interplanetary shocks, and it must therefore make the interpretation of a derived $Q(r,t)$ exceedingly difficult. With the exception of *Lee and Ryan's* [1986] study, a detailed study of shock acceleration at a dynamically evolving interplanetary shock has yet to be undertaken. Without such a study, many of the inferences and conclusions regarding the mechanism by which SEPs in gradual events are accelerated must be regarded as somewhat tentative and preliminary. Accordingly in this first report we have presented a study which eschews the complications of particle transport in the interplanetary medium and concentrates on the self-consistent injection, acceleration, and escape of ions at a dynamically evolving interplanetary shock. In many respects, this work therefore complements the theoretical work of Heras et al., Lario et al., Kallenrode and Wibberenz, and Kallenrode and Hatzky, and the observational work of, for example, *Cane et al.* [1988], *Domingo et al.* [1989], and *Reames et al.* [1996].

The basic model used here assumes a spherically symmetric solar wind into which a shock wave propagates. Both the wind and shock are modeled numerically on the basis of the standard hydrodynamic equations, and the IMF is modeled using the usual Parker solution. The shock strength and the compressed postshock flow field therefore evolve self-consistently and provide local values for the shock strength, Mach number, etc., which are needed to determine the accelerated energetic particle spectra. Suprathermal ions are injected at the shock and accelerated producing a local power law in energy. The local maximum particle energy accelerated at the shock is determined by equating the ion acceleration timescale and the shock dynamical timescale. The shock-accelerated particle distribution experiences both convection and diffusion in the radially expanding solar wind, which leads to the cooling and loss of energetic particles from the shock complex. The particles which escape into the interplanetary medium experience weak scattering as they propagate and do not return to the shock.

1. Since the results have been discussed in some detail in section 3, we merely enumerate our basic conclusions. These conclusions are based on a single example using a comparatively strong shock with an initial velocity at 0.1 AU of ~1500 km/s. The energy required for particles to be injected into the diffusive shock acceleration mechanism at quasi-parallel shocks is found to have little variation with heliocentric distance, ranging from ~5 to 3 keV. The injection ions require energies somewhat greater than that of thermal solar wind ions, which means that we require either a preexisting pool of energetic seed particles or an injection mechanism at the shock. However, the energy requirements are certainly not especially excessive and support the idea that thermal solar wind ions can be injected into the shock acceleration process. Specific injection mechanisms [*Malkov*, 1998] are not incorporated in the present model, although it is possible in principle. We have also not explored the possibly interesting distinction between accelerating preexisting seed particles (produced perhaps at flares) and thermal solar wind ions. Such a mixed population may have interesting implications in terms of understanding injection mechanism, efficiences, compositon, and abundances [*Mason et al.*, 1999]. Also, the role of possibly distinct plasma distributions, such as pickup ion He^+ and He^{++} within 2-3 AU, may illuminate differences between pickup ion and thermal solar wind injection [*Fränz et al.*, 1999].

2. Maximum particle energies accelerated at interplanetary shocks result from a competition between the decelerating shock speed, the weakening IMF, and the shock age. Unless a shock is accelerating, the maximum energy to which particles are accelerated at an interplanetary shock decreases monotonically with increasing radial distance. Nonetheless, substantial maximum particle energies are possible in the early stages of shock evolution. Energies of order 1 GeV are possible for young shock waves, and this decreases to ~100 MeV at 2 AU. Higher-energy particles tend to escape more easily from the shock complex, but a small number can remain trapped for an extended period.

3. In the shock precursor the radial mfp is found to be some 2 orders of magnitude smaller than the interplanetary mfp. This, of course, is a consequence of the streaming energetic ions driving unstable Alfvén waves in the vicinity of the shock. The small mfp at the shock supports the use of a

diffusive shock acceleration model. However, the larger interplanetary mfps also indicate the necessity of using a Boltzmann transport description away from the shock.

4. Although close to a power law, the accelerated particle spectrum experiences significant evolution as it is convected through the flow downstream of the shock. At the shock itself the accelerated spectrum has a convex or broken power law shape. The low-energy particle spectrum is flat ($\sim E^{-2}$) and steepens at high energies. The spectral steepening at high energies is a consequence of the greater (diffusive) mobility of very energetic particles and the ease with which they escape into interplanetary space from the shock complex. The evolution of the energetic particle spectrum shape through the postshock flow is from convex to concave. The spectral change in shape results from a combination of particle cooling and diffusive losses and gains at higher energies. The postshock distributions at different spatial locations therefore consist of a mixture of ions which were injected and accelerated in a variety of spatial locations and different epochs. The low-energy particles were accelerated "locally" at some earlier epoch whereas high-energy particles, because of their large diffusive length scales, could have been created at earlier or later times at a quite different stage of the shock evolution. It is unclear whether such mixing can be distinguished by comparing properties of high- and low-energy particles at a given position.

5. By contrast, the escaping omnidirectional particle spectrum, i.e., the spectrum located an escape distance ahead of the propagating shock, is in some sense the "mirror image" of the convex spectrum located at the shock. Instead of a convex spectrum, the escaping spectrum is concave: flat at high energies ($\sim E^{-2}$) and steeper at low energies for exactly the same reasons that the shock spectrum was convex. At early times, the low energy rolls off at ~10 MeV, but as the IMF weakens with increasing heliocentric distance, the lower-energy cut-off becomes smaller.

6. The spatial distribution of very energetic ions at and behind the shock flattens with time since, as the heliocentric distance increases, it becomes more difficult for these ions to remain trapped. Low-energy particles, however, remain trapped and cool in the shells within which they convect. Consequently, the radial profile for the intensity of low-energy ions increases monotonically with distance.

7. Preliminary calculations of the intensity profile as a function of time show that with the exception of the very lowest energy accelerated component (<20 keV), it possesses four distinct temporal regions: (1) A plateau corresponding to escaping particles which arrive at an observer well before the shock. The ions that comprise the plateau are not preexisting background energetic ions but are shock-accelerated particles which escaped from the acceleration region some time earlier and propagate ahead of the shock. This indicates that the particle composition in the plateau should reflect injection from the thermal solar wind material. (2) A period of exponential growth in the particle intensity. This period corresponds to the arrival of the shock precursor at a particular energy. (3) A peak followed by a decrease in particle intensity. If particles of a particular energy are no longer accelerated by a shock beyond some heliocentric distance (because the shock can no longer accelerate particles above a maximum energy beyond some radius), then the particle intensity peaks some time before the shock arrives at the observation point. The intensity decays rather rapidly thereafter because, although particles are trapped downstream of the shock, particles of such high energies are comparatively mobile and escape easily. If, instead, particles of a particular energy are still experiencing acceleration at the shock, then the peak in particle intensity coincides with the shock arrival time. The subsequent decay in intensity is faster for lower-energy particles than for particles of intermediate energy, because of diffusion in the post-shock flow. (4) A plateau downstream of the postshock flow, resulting from particle escape downstream of the postshock complex and propagation back to the observer.

Finally, we note that we have not, in this report, attempted to fit or directly relate our theoretical model to any set of observations. Instead, we have concentrated on the theoretical development of a model for particle acceleration and escape at a propagating interplanetary shock, and we have explored the predictive implications of the model. Most importantly, we have neglected to include detailed transport effects of the particles escaping from the shock and propagating in the interplanetary medium. However, even a cursory comparison of our results with some of the observations reviewed by, for example, *Reames* [1999] reveals that many of the characteristics predicted by our model are surprisingly similar, these ranging from broken power law spectra to maximum energies, to the forms of intensity profiles, etc. The relating of this model to specific observations will be pursued elsewhere (W. Rice et al., manuscript in preparation, 2000).

Acknowledgments. The support of NSF grants ATM-9713432 and ATM-9713223 and NASA awards NAG5-7796 and NAG5-5054 is gratefully acknowledged.

Janet G. Luhmann thanks May-Britt Kallenrode and another referee for their assistance in evaluating this paper.

References

Axford, W.I., E. Leer, and G. Skadron,The acceleration of cosmic rays by shock waves, *Conf. Pap. Int. Cosmic Ray Conf., 15th, 11*, 132-137, 1977.

Bell, A.R., The acceleration of cosmic rays in shock fronts, I, *Mon. Not. Astron. Soc., 182*, 147-156, 1978a.

Bell, A.R., The acceleration of cosmic rays in shock fronts, II, *Mon. Not. Astron. Soc., 182*, 443-455, 1978b.

Blandford, R.D., and J.P. Ostriker, Particle acceleration by astrophysical shocks, *Astrophys. J., 221*, 269-280, 1978.

Bogdan, T.J., and H.J. Völk, Onion-shell model of cosmic-ray acceleration in supernova remnants, *Astron. Astrophys., 122*, 129-136, 1983.

Cane, H.V., Energetic particles in the solar wind: propagation, acceleration and modulation, *Conf. Pap. Int. Cosmic Ray Conf., 25th, 8*, 135-150, 1997.

Cane, H.V., The structure and evolution of interplanetary shocks and the relevance for particle-acceleration, *Nucl. Phys. B., 39A*, 35-44, 1995.

Cane, H.V., R.E. McGuire, and T.T. von Rosenvinge, 2 Classes of solar energetic particle events associated with impulsive and long-duration soft-X-ray flares, *Astrophys. J., 301*, 448-459, 1986.

Cane, H.V, D.V. Reames, and T.T. von Rosenvinge, The role of interplanetary shocks in the longitude distribution of solar energetic particles, *J. Geophys. Res., 93*, 9555-9567, 1988.

Domingo, V., B. Sanahuja, and A.M. Heras, Energetic particles, interplanetary shocks and solar activity, *Adv. Space Res., 9*(4), 191-195, 1989.

Drury, L.O'C., An introduction to the theory of diffusive shock acceleration of energetic particles in tenuous plasmas, *Rep. Prog. Phys., 46*, 973-1027, 1983.

Dryer, M., Interplanetary studies: Propagation of disturbances between the Sun and the magnetosphere, *Space Sci. Rev., 67*, 363-419, 1994.

Fränz, M., E. Keppler, U. Lauth, M.K. Reuss, G.M. Mason, and J.E. Mazur, Energetic particle abundances at CIR shocks, *Geophys. Res. Lett., 26*, 17-20, 1999.

Gloeckler, G., J. Geiss, E.C. Roelof, L.A. Fisk, F.M. Ipavich, K.W.

Ogilvie, L.J. Lanzerotti, R. von Steiger, and B. Wilken, Acceleration of interstellar pickup ions in the disturbed solar wind observed on Ulysses, *J. Geophys. Res., 99,* 17,637-17,643, 1994.

Gosling, J.T., The solar-flare myth, *J. Geophys. Res., 98,* 18,937-18,949, 1993.

Gosling, J.T., J.R. Asbridge, S.J. Bame, W.C. Feldman, R.D. Zwickl, G. Paschmann, N. Sckopke, and R.J. Hynds, Interplanetary ions during an energetic storm particle event: The distribution from solar wind thermal energies to 1.6 MeV, *J. Geophys. Res., 86,* 547-554, 1981.

Heras, A.M., B. Sanahuja, Z.K. Smith, T. Detman, and M. Dryer, The influence of the large-scale interplanetary shock structure on a low-energy particle event, *Astrophys. J., 391,* 359-369, 1992.

Heras, A.M., B. Sanahuja, D. Lario, Z.K. Smith, T. Detman, and M. Dryer, 3 Low energy particle events: Modeling the influence of the parent interplanetary shock, *Astrophys. J., 445,* 497-508, 1995.

Jokipii, J.R., Rates of energy gain and maximum energy in diffusive shock acceleration, *Astrophys. J., 313,* 842-846, 1987.

Kahler, S.W., Solar flares and coronal mass ejections, *Ann. Rev. Astron. Astrophys., 30,* 113-141, 1992.

Kahler, S.W., N.R. Sheeley, R.A. Howard, M.J. Koomen, D.J. Michels, R.E. McGuire, T.T. von Rosenvinge, and D.V. Reames, Associations between coronal mass ejections and solar energetic proton events, *J. Geophys. Res., 89,* 9683-9693, 1984.

Kallenrode, M.-B., and R. Hatzky, Energetic particle events at traveling interplanetary shocks: Modeling between 20 keV and 500 MeV, *Conf. Pap. Int. Cosmic Ray Conf., 26th, 6,* 324-327, 1999.

Kallenrode, M.-B., and G. Wibberenz, Propagation of particles injected from interplanetary shocks: A black box model and its consequences for acceleration theory and data interpretation, *J. Geophys. Res., 102,* 22,311-22,334, 1997.

Krymsky, G.F., A regular mechanism for the acceleration of charged particles on the front of a shock wave, *Dok. Akad. Nauk. SSSR, 234,* 1306-1308, 1977.

Lagage, P.O., and C.J. Cesarsky, Cosmic-ray shock acceleration in the presence of self excited waves, *Astron. Astrophys., 118,* 223-228, 1983.

Lario, D., B. Sanahuja, and A.M. Heras, Energetic particle events: Efficiency of interplanetary shocks as 50 keV < E < 100 MeV proton accelerators, *Astrophys. J., 509,* 415-434, 1998.

Lee, M.A., Coupled hydrodynamic wave excitation and ion-acceleration at interplanetary traveling shocks, *J. Geophys. Res., 88,* 6109-6119, 1983.

Lee, M.A., and J.M. Ryan, Time-dependent coronal shock acceleration of energetic solar-flare particles, *Astrophys. J., 303,* 829-842, 1986.

Leske, R.A., J.R. Cummings, R.A. Mewaldt, E.C. Stone, and T.T. von Rosenvinge, Measurements of the ionic charge states of solar energetic particles using the geomagnetic-field, *Astrophys. J., 452,* L149-L152, 1995.

Luhn, A., B. Klecker, D. Hovestadt, and E. Mobius, The mean ionic charge state of silicon in He-3 rich events, *Adv. Space Res., 4*(2/3), 161-164, 1984.

Luhn, A., B. Klecker, D. Hovestadt, and E. Mobius, The mean ionic charge state of silicon in He-3-rich solar-flares, *Astrophys. J., 317,* 951-955, 1987.

Malkov, M.A., Leakage from quasi-parallel collisionless shocks: Implications for injection and shock dissipation, *Phys. Rev. E. Stat. Phys. Plasmas Fluids Relat. Interdiscip. Top., 58,* 4911-4928, 1998.

Mason, G.M., G. Gloeckler, and D. Hovestadt, Temporal variations of nucleonic abundances in solar-flare energetic particles events, 2, Evidence for large-scale shock acceleration, *Astrophys. J., 280,* 902-916, 1984.

Mason, G.M., J.E. Mazur, M.D. Looper, and R.A. Mewaldt, Charge-state measurements of solar energetic particles observed with SAMPEX, *Astrophys. J., 452,* 901-911, 1995.

Mason, G.M., et al., Particle acceleration and sources in the November 1997 solar energetic particle event, *Geophys. Res. Lett., 26,* 141-144, 1999.

McKenzie, J.F., and H.J. Volk, Non-linear theory of cosmic ray shocks including self-generated alfvén waves, *Astron. Astrophys., 116,* 191-200, 1982.

McKibben, R.B., Azimuthal propagation of low-energy solar-flare protons as observed from spacecraft very widely separated in solar azimuth, *J. Geophys. Res., 77,* 3957-3984, 1972.

Moraal, H., and W.I. Axford, Cosmic-ray acceleration in supernova blast waves, *Astron. Astrophys., 125,* 204-216, 1983.

Ng, C.K., D.V. Reames, and A.J. Tylka, Effect of proton-amplified waves on the evolution of solar energetic particle composition in gradual events, *Geophys. Res. Lett., 26,* 2145-2148, 1999.

Oetliker, M., B. Klecker, D. Hovestadt, G.M. Mason, J.E. Mazur, R.A. Leske, R.A. Mewaldt, J.B. Blake, and M.D. Looper, The ionic charge of solar energetic particles with energies of 0.3-70 MeV per nucleon, *Astrophys. J., 477,* 495-501, 1997.

Parker, E.N., Dynamics of the interplanetary gas and magnetic fields, *Astrophys. J., 123,* 664-676, 1958.

Reames, D.V., and R.G. Stone, The identification of solar He-3 rich events and the study of particle acceleration at the sun, *Astrophys. J., 308,* 902-911, 1986.

Reames, D.V., Energetic particles from impulsive solar-flares, *Astrophys. J. Suppl. S., 73,* 235-251, 1990.

Reames, D.V., Coronal element abundances derived from solar energetic particles, *Adv. Space Res., 14(4),* 177-180, 1993.

Reames, D.V., Coronal abundances determined from energetic particles, *Adv. Space Res., 15*(7), 41-51, 1995.

Reames, D.V., Particle acceleration at the Sun and in the heliosphere, *Space Sci. Rev., 90*(3/4), 413-491,1999.

Reames, D.V., L.M. Barbier, and C.K. Ng, The spatial distribution of particles accelerated by coronal mass ejection-driven shocks, *Astrophys. J., 466,* 473-486, 1996.

Reames, D.V., S.W. Kahler, and C.K. Ng, Spatial and temporal invariance in the spectra of energetic particles in gradual solar events, *Astrophys. J., 491,* 414-420, 1997.

Ruffolo, D., Effect of adiabatic deceleration on the focused transport of solar cosmic rays, *Astrophys. J., 442,* 861-874, 1995.

Ruffolo, D., Interacting and escaping solar energetic particles, *Conf. Pap. Int. Cosmic Ray Conf., 25th, 9,* 109-134, 1997.

Shimada, N., Diffusive shock acceleration process of electrons in the solar wind, Ph.D. thesis, Univ. of Tokyo, Tokyo, 1998.

Tan, L.C., G.M. Mason, F.M. Ipavich, G. Gloeckler, R.D. Zwickl, and S.J. Bame, Energetic proton and helium fluxes associated with interplanetary shocks and their relation to the solar wind composition, *J. Geophys. Res., 91,* 1009-1018, 1986.

Terasawa, T., K. Maezawa, M. Hoshino, N. Shimada, T. Mukai, Y. Saito, T. Yamamoto, S. Kokubun, B. Wilken, and T. Doke, Observation of a cosmic-ray-modified interplanetary shock, *Conf. Pap. Int. Cosmic Ray Conf., 26th, 6,* 528-531, Salt Lake City, Utah, 1999.

Tylka, A.J., P.R. Boberg, J.H. Adams, L.P. Beahm, W.F. Dietrich, and T. Kleis, The mean ionic charge state of solar energetic Fe ions above 200 MeV per nucleon, *Astrophys. J., 444,* L109-L113, 1995.

Tylka, A.J., D.V. Reames, and C.K. Ng, Observations of systematic temporal evolution in elemental composition during gradual solar energetic particle events, *Geophys. Res. Lett., 26,* 2141-2144, 1999.

Völk, H.J., L.A. Zank, and G.P. Zank, Cosmic-ray spectrum produced by supernova-remnants with an upper limit on wave dissipation, *Astron. Astrophys., 198,* 274-282, 1988.

Webb, G.M., G.P. Zank, C.M. Ko, and D.J. Donohue, Multidimensional greens-functions and the statistics of diffusive shock acceleration, *Astrophys. J., 453,* 178-206, 1995.

Zank, G.P., Interaction of the solar wind with the local interstellar medium: A theoretical perspective, *Space Sci. Rev., 89*(3/4), 413-688, 1999.

W. K. M. Rice and G. P. Zank, Bartol Research Institute, University of Delaware, Newark, DE, 19716. (rice@bartol.udel.edu; zank@bartol.udel.edu)

C. C. Wu, 5367 Mad River Lane, Columbia, MD 21044. (ccwu@bartol.udel.edu)

(Received December 21, 1999; revised April 20, 2000; accepted April 21, 2000.)